

Strain-induced modification of magnetic structure and new magnetic phases in rare-earth epitaxial films

C DUFOUR¹, K DUMESNIL¹ and PH MANGIN²

¹Laboratoire de Physique des Matériaux, Université H. Poincaré-Nancy I, BP 239, 54506 Vandoeuvre les Nancy Cédex, France

²Laboratoire Léon Brillouin, CEA Saclay, 91000 Gif sur Yvette Cédex, France

E-mail: mangin@dsm-mail.saclay.cea.fr; dufour@lpm.u-nancy.fr; dumesnil@lpm.u-nancy.fr

Abstract. Rare earths exhibit complex magnetic phase diagrams resulting from the competition between various contributions to the magnetic energy: exchange, anisotropy and magnetostriction. The epitaxy of a rare-earth film on a substrate induces (i) a clamping to the substrate and (ii) pseudomorphic strains. Both these effects are shown to lead to modifications of the magnetic properties in (0 0 1)Dy, (0 0 1)Tb and (1 1 0)Eu films. In Dy and Tb films, spectacular variations of the Curie temperature have been evidenced. Additionally, Tb films exhibit a new large wavelength magnetic modulation. In Eu films, one of the helical magnetic domains disappears at low temperature whereas the propagation vectors of the other helices are tilted. The link between structural and magnetic properties is underlined via magnetoelastic models. Moreover, molecular beam epitaxy permits the growth of Sm in a metastable dhcp phase. The magnetic structure of dhcp Sm has been elucidated for the first time. In this review, neutron scattering is shown to be a powerful technique to reveal the magnetic structures of rare-earth films.

Keywords. Magnetic nanostructures; neutron scattering; Curie temperature.

PACS No. 75.30.-m

1. Introduction

Beyond the strong interest in the area of device development, magnetic nanostructures are known to exhibit unique and exciting fundamental properties [1]. Among the magnetic nanostructures, those involving rare-earth metals are of particular interest because of the modulated magnetic phases and the magnetostrictive properties present in the bulk [2].

In bulk lanthanide elements, the combination of weak exchange and anomalous large crystal field and magnetostrictive interactions, arising from the strong spin-orbit coupling and the highly non-spherical $4f$ charge distribution, results in comparable magnitude for exchange and crystal field energies. This situation, as well as the long range and oscillating character of the indirect exchange interaction, leads

to a large number of exotic modulated structures. Neutron diffraction has been shown to be a unique tool to elucidate these magnetic modulated structures.

In epitaxial films, one crucial feature is that the crystal lattice is generally distorted, either by pseudomorphic growth on other materials or by clamping to the thick (0.4 mm) substrate. Therefore, the modulated magnetic order, intimately correlated with the geometry of the Fermi surface, can be modified in epitaxial films [3]. Moreover, the magnetic properties can be modified via the magnetoelastic interaction.

Another important feature is that the epitaxial process can lead to the growth of a metastable phase, i.e. to the growth of a film with a crystallographic structure different from the bulk one in normal temperature and pressure conditions. Both exchange and crystal field effects being very sensitive to the crystal structure, the determination of the magnetic structure of such a metastable phase is of great interest for a better understanding of rare-earth magnetism.

The aim of this paper is to demonstrate the occurrence of new magnetic structures in rare-earth thin films (10 to 700 nm) grown by molecular beam epitaxy on (110) sapphire substrates and to underline the link between these new magnetic properties and the structural aspects. We will first show that, in the heavy rare earth Dy and Tb, in which the magnetostrictive energy drives the ferromagnetic transition, the structural distortion in thin films induces significant shifts of the Curie temperature [4–6]. Moreover, in Tb, the clamping to the substrate leads to the occurrence of a large wavelength magnetic modulation [7,8]. In Eu films, this clamping induces a unique magnetic ordering at low temperature [9,10]. Finally, Sm has been grown with a crystallographic order different from the bulk (dhcp) and the corresponding magnetic order has been evidenced [11]. Most of the results have been obtained from neutron diffraction: This demonstrates that the technique thus remains powerful for the determination of magnetic structures in films in the 50–1000 nm range.

2. Elaboration of the films and structural characterization

The samples were prepared by molecular beam epitaxy in a vacuum chamber whose base pressure was about $4 \cdot 10^{-11}$ Torr. They were grown on a 0.4 mm thick (110) sapphire substrate which was degreased and then heated to 850°C for 1 h in the growth chamber. Following the method proposed by Kwo *et al* [12] for rare earth with hexagonal structure, the substrate was first covered by a 50 nm thick bcc Nb buffer layer deposited at 800°C. The growth direction is [110]. When Nb is deposited at high temperature, the surface is reconstructed due to chemisorbed oxygen. The rare earths are then evaporated from an effusion cell (Sm, Eu, Er) or an electron gun (Dy, Tb, Y, Nd) on the substrate kept at a temperature varying between 150°C and 450°C depending on the melting temperature of the metal.

The aim is to study the magnetic properties of Dy, Tb, Eu and Sm epitaxial films. In order to either induce pseudomorphic strains or to initiate a growth in a crystalline structure different from the bulk, these magnetic rare earths have been grown on different templates. Bulk Dy, Tb, Er and Y present an hcp structure. Dy films have been grown on a 50 nm thick Y or Er template, and then recovered with a 50 nm thick Y or Er layer. Tb films have grown either directly on Nb or on a Y template.

To initiate the dhcp growth of Sm, a thin (001)Nd template layer (2 nm thick) was grown on the (110)Nb buffer [13]. Let us recall that bulk Nd is dhcp whereas bulk Sm exhibits a nine hexagonal close-packed plane stacking sequence. From *in-situ* reflection high-energy electron diffraction (RHEED), the in-plane symmetry is hexagonal for all hexagonal rare earths (Dy, Tb, Y, Er, Sm, Nd) deposited on (110)Nb. The growth direction is [001] and the epitaxial relationships are: (110)Al₂O₃||[(110)Nb]||[(001)RE] with [002]Nb||[1̄10]RE and [1̄10]Nb||[100]RE where RE = hexagonal rare earth = Dy, Tb, Er, Y, Sm or Nd.

Eu is a light rare earth which in amazing contrast with most of the rare-earth elements crystallizes in a bcc lattice. This behaviour is commonly attributed to the occupancy of the 5*d* electronic shell that differs from the other rare earths because of the divalent character of Eu. 2D hexagonal layers of Eu of a few nanometers are obtained when Eu is deposited directly on the (110)Nb buffer deposited at 800°C. This hexagonal surface always favours, after relaxation, a 3 domain (110)Eu structure.

However, starting from a pure (110)Nb surface, obtained in burying oxygen by a 150°C Nb overdeposit, we can fabricate single domain bcc (110)Eu layers of high crystal quality [14]. The epitaxial relationships, deduced from RHEED patterns, are the following:

$$[001]Nb||[001]Eu \quad \text{and} \quad [\bar{1}10]Nb||[\bar{1}10]Eu.$$

Finally, a 50 nm thick layer (either niobium or yttrium) was deposited on the top of all the samples, in order to avoid further oxidation of the rare earth.

For the whole set of films, RHEED patterns exhibit thin and continuous streaks, which confirm the 2D coherence and the single crystal quality of the deposited layers [13,14]. X-ray diffraction experiments confirm the high crystal quality of the samples. All the films are single crystals. The coherence length along the growth direction is around 80 nm for hexagonal rare earth and 50 nm for (110)Eu. The mosaic spread was estimated to vary between 0.2 and 0.4° for hexagonal (001) rare earths and between 0.2° and 1° for (110)Eu.

3. Shift of Curie temperature in Dy(001) films [4–6]

Bulk Dy orders from the paramagnetic to the helical state at $T_N = 179$ K. Below this temperature, the magnetic moments are in the basal plane and the helix wave vector is along the *c*-axis. The turn angle decreases from 44° just below T_N to 26° at $T_C = 89$ K where it drops to 0° [15,16]. This drop corresponds to the occurrence of a ferromagnetic phase with the moments orientated along the *a*-axis.

The ferromagnetic transition is known to be driven by magnetoelastic effects [17] which balance the exchange interaction provided by the conduction electrons. Three symmetry strains have to be taken into account: α_1 strains corresponding to a pure expansion, α_2 strains corresponding to a cylindrical distortion and γ strains corresponding to an orthorhombic distortion [18]. Only α strains are linked to the *c* parameter which is not involved in the γ strain.

In the paramagnetic phase, the neutron diffraction peaks are purely nuclear and the magnetic scattering is diffuse. The diffraction pattern in the helical phase is

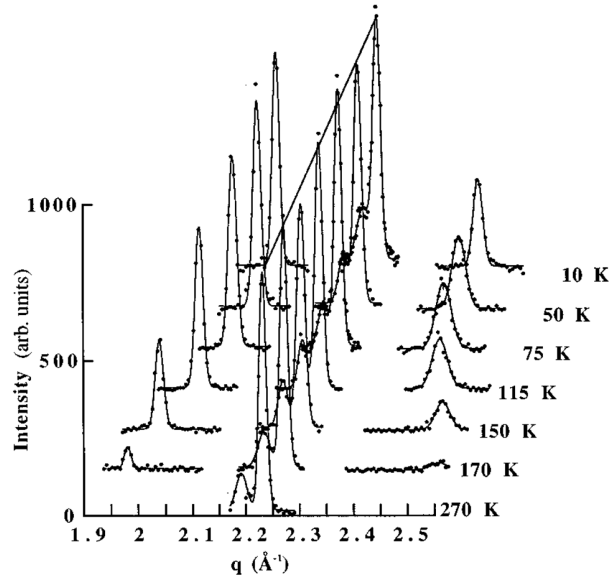


Figure 1. Neutron scattering spectra measured at different temperatures along the c^* direction around the (002) reflection for a Y/Dy 60 nm/Y trilayer.

characterized by the occurrence of magnetic satellites on each side of the nuclear peaks. The ferromagnetic transition leads to the disappearance of these satellites and to the simultaneous increase of the nuclear peak intensity.

A set of neutron scattering spectra from a 60 nm thick Dy film grown between two Y films around the (002) reflection is shown in figure 1 (G4.3 triple axis spectrometer, LLB, France). The two central peaks are the Y and Dy nuclear peaks. Their relative intensity is due to the small nuclear coherent scattering amplitude of neutron in Y compared to that in Dy. The satellites located on both sides due to the helical magnetic order appear at 179 K and persist down to 10 K. This indicates that the helical phase is stable down to low temperature and that, contrary to the bulk, there is no ferromagnetic transition. On the contrary, in Dy films grown between Er layers, the opposite effect is observed: the range of existence of the helical phase is reduced and the Curie temperature is increased.

To summarize the effects observed in Dy films grown on Y or on Er, figure 2 presents the variation of the Curie temperature T_C as a function of the ϵ_{33} strain for a set of Dy films grown either between Y or between Er. The strain ϵ_{33} is perpendicular to the plane growth one measured at 300 K from X-ray diffraction. The sign of the strain depends on the buffer layer. In fact, when Dy is epitaxially grown on Y, this leads to a positive strain in the basal plane and to a negative one along the c direction. On the contrary, an epitaxial growth of Dy on Er leads to strains of opposite signs in Dy. Moreover, the absolute value of the strain depends on the film thickness. The thinner is the film, the larger is the absolute value of the strain. From figure 2, one can conclude that the Curie temperature varies continuously with the strain. However, this evolution is not linear: T_C increases only slowly for $\epsilon_{33} > 0$ but decreases more rapidly when $\epsilon_{33} < 0$. When the perpendicular

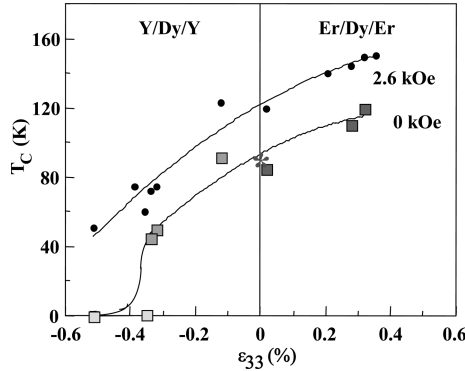


Figure 2. Variation of T_C (values measured under 2.6 kOe (filled circles) and obtained by extrapolation to 0 kOe (squares)) for Dy films grown between Y or Er vs. the strain ε_{33} . The lines are guides to the eyes.

strain is negative and its absolute value is larger than 0.4, the ferromagnetic phase is suppressed.

A careful study of the variation of the c lattice parameter has been undertaken as a function of temperature. For the Dy films presenting a ferromagnetic transition, a discontinuous expansion of this parameter is observed at T_C , as in bulk Dy, which is the signature of a step of the α strains. However, the amplitude of the step is smaller when Dy is grown on Er and larger when it is grown on Y. The amplitude of the expansion along the c -axis is related to the contribution of the α strains to the driving energy and corresponds to the difference between the magnetostrictive energies in the ferromagnetic and helical phases.

Moreover, it has been shown that the in-plane orthorhombic distortion (γ distortion), that occurs around T_C in the bulk Dy, is also observed in the epitaxial Dy films but is progressive: it is partially clamped. Finally, figure 3 shows the thermal variation of the turn angle for bulk Dy and various Dy films. As in bulk, the turn angle in Dy films decreases with temperature, which is interpreted by superzone gaps in the Fermi surface, due to magnetic ordering. This reveals the decrease of the energy barrier, which makes the ferromagnetic transition possible. What is very interesting is that the values of the turn angle are significantly shifted compared to the bulk values. For Dy layers between Y layers, it is larger than the bulk value, whereas for Dy layers between Er layers, it is smaller. Moreover, the shift of the turn angle is observed still at high temperature, near T_N , where the magnetoelastic effects are negligible. It could therefore be explained by a modification of the exchange energy barrier due to modifications of the Fermi surface of Dy by the epitaxial strain. Note finally that the turn angle for the Y/Dy 60 nm/Y film never drops to zero because the ferromagnetic transition is suppressed.

A magnetoelastic model permits to explain the main features of the shift of T_C when Dy is grown either on Y or on Er [5]. The strain at equilibrium has been determined first. Then the thermal variations of the various magnetic energies have been calculated in the ferromagnetic and helical phases and energy diagrams have been elaborated. The ferromagnetic transition occurs when the sum of the energies in the helical phase equals the sum of the energies in the ferromagnetic

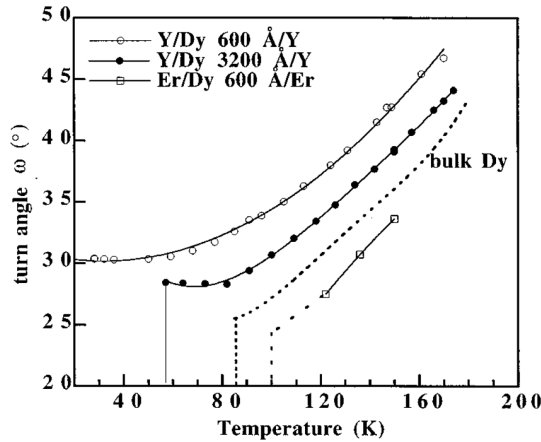


Figure 3. Thermal variation of the turn angle between Dy moments in Y/Dy/Y (60 nm Dy film: filled circles, 320 nm Dy film: open circles) and Er/Dy/Er trilayers (60 nm Dy film: squares). The dotted line represents the variation in bulk Dy.

phase. The values of the Curie temperature obtained with this method are in good agreement with experimental data. The fact that the Curie temperature is an increasing function of the ϵ_{33} strain and that this function is not linear can be well-understood. In Y/Dy/Y, all the effects are in favour of a decreasing T_C : the signs of the α strains are opposite to those observed in bulk, the γ distortion is reduced and the exchange energy barrier is larger than in bulk. In Er/Dy/Er trilayers, the increase of T_C is disfavoured by the clamping but is rather favoured by the epitaxial α strains and by the lowered exchange energy barrier.

4. Large wavelength magnetic modulation in (001)Tb films [7,8]

Bulk hcp Tb presents the same sequence of magnetic phases as the bulk Dy but with significant differences [19–21]: (i) the Néel temperature is higher, i.e., $T_N = 230$ K, (ii) the helical phase is stable on a very reduced temperature range: the first-order ferromagnetic transition occurs at $T_C = 220$ K, (iii) the turn angle between magnetic moments of successive basal planes is 21° just below T_N and (iv) because of the shape of the electronic cloud and of the consequent anisotropy, the magnetic moments lie in the basal plane along the b -axis.

Neutron scattering spectra under zero magnetic field from a 700 nm thick Tb film are shown in figure 4a for temperatures between 230 and 216 K and in figure 4b for temperatures between 214 and 20 K (G4.3 triple axis spectrometer, LLB, France). At 230 K, the neutron diffraction pattern exhibits the (002) nuclear peak at $q = 2.21 \text{ \AA}^{-1}$. Around 229 K, two satellites (referred to as ‘helix’ in figure 4a) emerge on each side of the (002) peak. These satellites are due to the magnetic helix which develops in bulk Tb with a wave vector parallel to the c -axis. Because their intensity is related to the square of the average magnetic moments, it increases

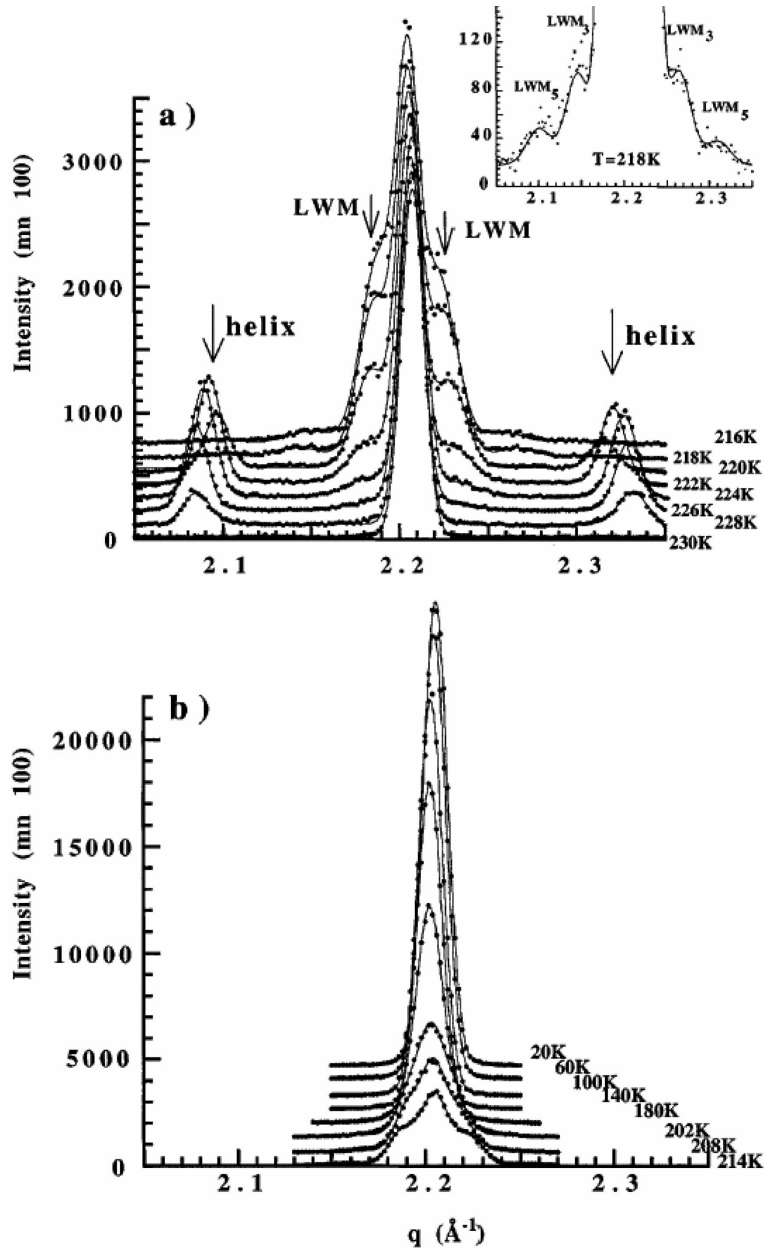


Figure 4. Neutron scattering spectra collected at different temperatures along the c^* direction around the (002) reflection for a 700 nm thick Tb film: (a) $T = 230, 228, 226, 224, 222, 220, 218$ and 216 K from the bottom to the top; (b) $T = 214, 208, 202, 130, 140, 100, 60$ and 20 K from the bottom to the top. The inset shows the occurrence of the third- and fifth-order satellites of LWM phase at 218 K.

continuously when the temperature decreases. The helix is stable down to about 220 K; then the satellite intensity drops abruptly. This behaviour is similar to the one observed in bulk Tb. However, contrary to bulk Tb, the magnetic intensity is not directly transferred from the helix satellites to the (002) Bragg peak but it is transferred to a new set of satellites. These satellites are very close to the (002) Bragg peak, but far enough to keep the intensity of this peak unchanged. They reveal an unexpected magnetic modulation of small wave vector and therefore of large wavelength, which can be estimated to be 290 Å at 220 K. The intensity of these large wavelength modulation peaks (referred to as LWM in figure 4) increases when the temperature decreases. At 222 and 220 K, both magnetic modulations, the classical helical modulation and the large wavelength modulation, coexist.

A careful examination of the diffraction pattern at 218 K shows that the large wavelength modulation gives rise to several other additional satellites referred to as LWM₃ and LWM₅ (see the inset of figure 4a). These peaks reveal that the modulation is not sinusoidal but has a square shape. When the temperature decreases, the LWM main satellites become closer and closer to the (002) peak and progressively merge into that peak. This last process is clearly visible from 214 to 208 K (figure 4b) and, below this temperature, it continues to be manifested by the simultaneous increase of the (002) peak intensity and the reduction of its width. Below 180 K, the width of the Bragg peak remains constant down to low temperature: the sample presents a long range ferromagnetic order. When increasing the temperature again, the process is reversible: the LWM and helical modulation successively reappear. However, the results present some hysteresis, as expected from a first-order transition.

A very similar behaviour was observed from a 200 nm thick Tb film and from a 40 nm thick one deposited between two Y layers. This last sample exhibits the successive phases with a shift of the transition temperature. The larger stability of the helical phase (i.e. the decrease of T_C) in this sample is consistent with the reduced c parameter due to the epitaxial strains, which increase the in-plane parameters of Tb deposited between Y layers. Correlatively, the turn angle is enhanced in agreement with the relation between the turn angle and the stability of the helical phase. Evolutions of the c parameters and of the turn angles are reported in figure 5. Finally, we have determined the stability of both magnetic modulations under an external magnetic field. The magnetic field needed to destroy the LWM phase and to induce ferromagnetic long range order is of the same order of magnitude as the one necessary to destroy the helical phase.

Concerning the origin of this LWM phase, we suggest that it is constituted by the stacking along the c -axis of ferromagnetic blocks with in-plane magnetization. Assuming that the resulting moment in each block is aligned along one of the equivalent b easy axes and that the magnetization rotates by 60° between two consecutive blocks, we can deduce the block thickness from the magnetic period. In the 700 nm film, the block thickness would increase from 15 to 41 atomic planes when the temperature decreases. The main argument for this block rotation is the occurrence of third- and fifth-order harmonics that we observed at 218 and 216 K (inset of figure 4a) and which are typical of a square profile. This magnetic arrangement permits us to obtain a compromise between the lowest energy configuration in the Tb film, that would be the long range ferromagnetic order accompanied by magne-

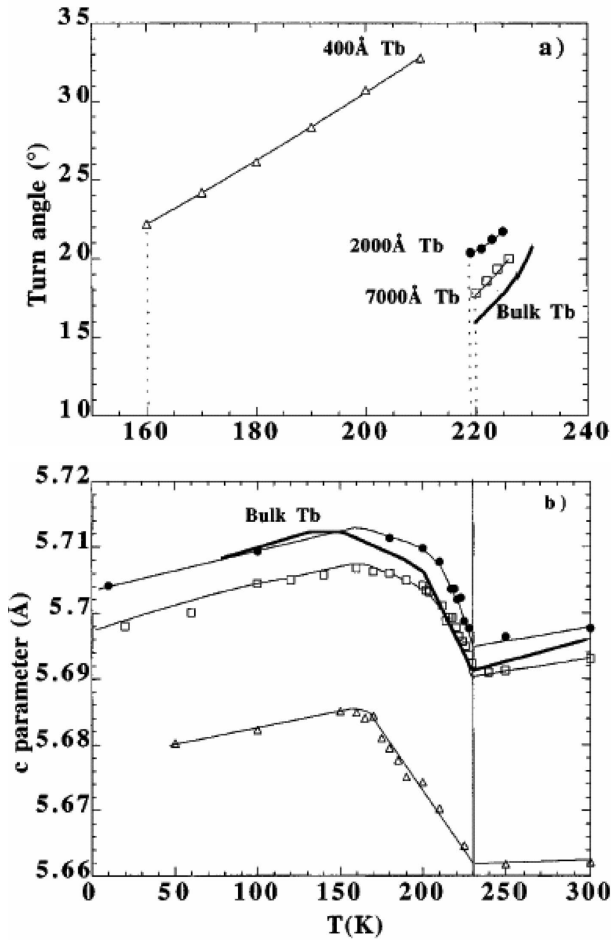


Figure 5. Thermal variation of the Tb turn angle (a) and of the Tb *c* parameter for 700 nm (open squares), 200 nm (filled circles) and 40 nm (open triangles) Tb films.

tostrictive lattice strains, and a configuration limiting the lattice strains in the other non-magnetic layers; the strains in these layers would only lead to a cost in elastic energy. Because of the clamping between the Tb and the non-magnetic buffer lattices, a long-range ferromagnetic order would then increase the total elastic energy in the sample. The ‘block by block’ rotation of the magnetization permits us to keep the short-range ferromagnetic ordering for most of the atoms in Tb and to reduce the total elastic energy. When the temperature decreases, the magnetic anisotropy becomes stronger and it no longer allows the existence of domain walls between the ferromagnetic blocks. This drives the long-range ferromagnetic arrangement. In the same way, the LWM phase is not observed in Dy films because of the larger magnetic anisotropy of Dy at the ferromagnetic transition.

5. Rotation of magnetic propagation vectors induced by lattice clamping in (1 1 0)Eu films [9,10]

Bulk Eu metal orders at $T_N = 90$ K [22] in a helical structure with magnetic propagation vectors parallel to the $\langle 001 \rangle$ axes of the bcc structure [23], giving three different magnetic domains: D_1 , D_2 and D_3 . The magnetic moments are aligned ferromagnetically within the $\{001\}$ planes perpendicular to the magnetic propagation vectors. The phase transition to the incommensurate helical structure has been reported to be first order [24–27], accompanied by a tetragonal distortion of the lattice, with expansion along the propagation direction [26].

The magnetic behaviour of a 375 nm thick (1 1 0)Eu film is presented first. Figure 6 shows the thermal dependence of (a) the magnetic peak intensities and (b) the angle of the magnetic propagation directions for the three helices, relative to the original $\langle 001 \rangle$ propagation directions in bulk Eu. The magnetic intensity (figure 6a) was measured by resonant X-ray magnetic scattering (RXMS at BM28 beamline ESRF, France). The magnetic wavelength and its temperature dependence, similar for the three helices and very close to bulk Eu, are not presented here.

In this film, the ordering temperature is close to the bulk one (90.4 K). However, their intensities do not exhibit any discontinuous jump at T_N , which may imply that the transition is no longer of first order. Moreover, the relative intensities of the magnetic peaks, reflecting the domain populations, vary strongly with temperature. When decreasing the temperature below 60 K, the helix propagating in the sample plane (domain D_3) vanishes to the benefit of the other two and is completely suppressed below 40 K. Upon increasing the temperature again, D_3 is not restored until the temperature reaches 70 K. Thus the three magnetic helices are no longer equally populated over the entire temperature range.

The most puzzling result is however obtained when considering the magnetic propagation vectors, as deduced from the positions in reciprocal space of pairs of magnetic satellites (figure 6b). The magnetic propagation directions are defined by the angle β with respect to the $\langle 001 \rangle$ crystal axes. While the in-plane magnetic wave vector κ_3 remains parallel to the $[001]$ cubic direction ($\beta = 0$), κ_1 and κ_2 are perpendicular to $[001]$ but tip away from the cubic directions as the temperature is decreased. They tend towards each other and towards the $[110]$ growth direction (schematic in figure 6b). This behaviour is consistent with the broken cubic symmetry, since $[001]$ is the only cubic direction lying in the growth plane, whereas $[100]$ and $[010]$ are both oriented at 45° relative to the growth plane.

For thicknesses ranging from 37 to 750 nm, the temperature below which the D_3 domain disappears and the value of the β tilt angle at 10 K for the two remaining propagation vectors κ_1 and κ_2 both increase when the thickness decreases. Thus, the symmetry breaking is more pronounced in thinner films. These strong deviations from the bulk Eu magnetic behaviour are true for relatively thick Eu films (750 nm).

A detailed structural investigation has been performed in measuring the interplanar distances along three perpendicular directions (1 1 0), (1 $\bar{1}$ 0) and (0 0 2), as a function of increasing temperature. The in-plane distortion appears isotropic and $a_{(002)}$ is not presented. Figure 7 displays the equivalent parameters, $a_\perp = a_{(110)}$ and $a_\parallel = a_{(1\bar{1}0)}$ for three different Eu thicknesses. Above a clamping temperature

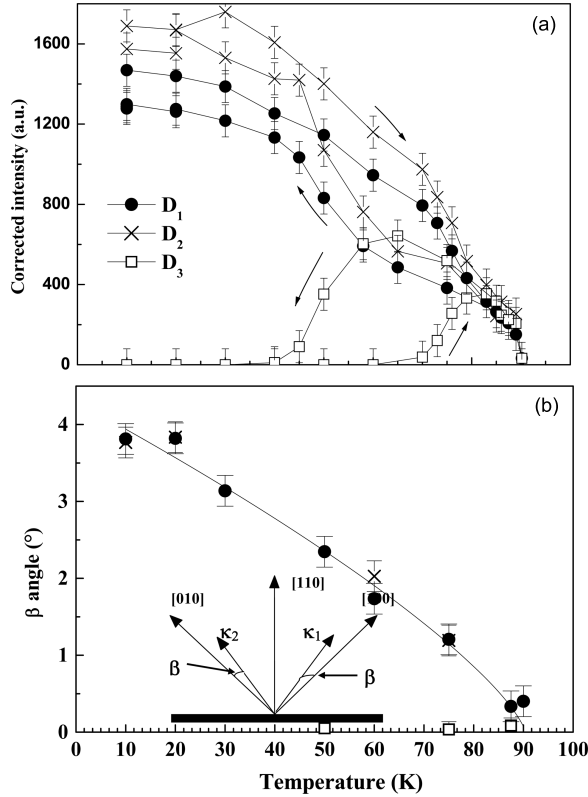


Figure 6. Temperature-dependent magnetic behaviour measured by RXMS in a 375 nm (1 1 0)Eu film. (a) Magnetic intensities associated with the three magnetic domains, corrected for the geometrical factors in the dipolar resonant scattering cross-section and for self attenuation. (b) Magnetic propagation directions, defined by the β angle between the wave vector and the $\langle 001 \rangle$ axes. The solid curves are only guides to the eyes.

T_{cl} , a_{\perp} and a_{\parallel} approximately match the bulk Eu values and decrease continuously with temperature for all three films. The corresponding thermal expansion coefficient is in perfect agreement with data on bulk Eu [26]. However, below T_{cl} , the in-plane lattice parameter leaves the thermal reduction and is almost constant down to 10 K. The clamping temperatures are estimated to be 250, 150 and 125 K respectively in the 75, 375 and 750 nm films. Note however that the clamping of the in-plane parameters does not affect the bulk-like temperature dependence of the perpendicular parameter, because the Poisson coefficient for Eu is small (0.15). This clamping effect, occurring above the Eu magnetic ordering temperature, is probably related to interactions between the Eu deposited film and the underlying (Nb buffer layer + sapphire substrate) system, which has a significantly smaller thermal expansion coefficient. Above T_{cl} , the Eu cubic lattice contracts independently of the underlying system. Below T_{cl} , the Eu lattice is clamped to the underlying system and therefore distorts with decreasing temperature.

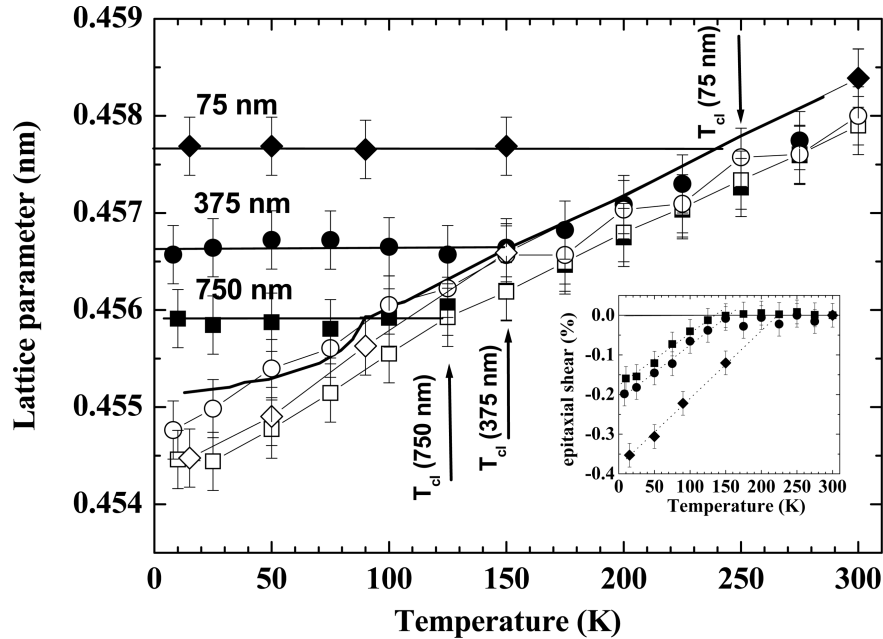


Figure 7. Thermal variations of the Eu equivalent lattice parameters along the $[110]$ (a_{\perp}) and $[1\bar{1}0]$ (a_{\parallel}) directions for three films: 75 nm (diamonds), 375 nm (circles) and 750 nm (squares). For each film, filled symbols are used for a_{\parallel} and open symbols for a_{\perp} . The lines are guides to the eyes and the bold curve corresponds to bulk Eu [26]. Inset: Thermal variations of the shear strain for the three samples.

This in-plane clamping gives rise to two main features: (i) the occurrence of an ε_{xy} shear: $\varepsilon_{xy}(T) = [a_{(110)} - a_{(1\bar{1}0)}]/2a$, where a is the bulk lattice parameter at the temperature T ; (ii) a dissymmetry between the tensile deformations: $\varepsilon_{zz} = \varepsilon_{\parallel}$, while $\varepsilon_{xx} = \varepsilon_{yy} = [\varepsilon_{\perp} + \varepsilon_{\parallel}]/2$. The amplitude of the ε_{xy} shear increases as the temperature and the film thickness decrease (inset in figure 7).

For symmetry reasons, the rotation of the magnetic wave vectors κ_1 and κ_2 in the xy plane is undoubtedly related to the ε_{xy} shear deformation. Two possible mechanisms may be invoked:

(i) The lattice strains act on the magnetic wave vectors via modifications of the Fermi surface and, subsequently, of the exchange interaction. This is the most direct way to modify the wave vectors. Following the formalism proposed by Bertaut [28], we have shown that the modification of exchange constants driven by the occurrence of strains lead to a corrective term to the exchange energy. In fact, the calculations demonstrate that a shear strain can tip the wave vector directions via modification of the exchange constants and that the tip angle is proportional to the strain. The weakness of this first approach is however, that the calculated value of β is different from zero at T_N since the lattice strains appear above T_N , while the experimental β obviously starts from zero at T_N .

(ii) The lattice strains alter the directions of the magnetic moments via magnetoelastic interactions. In this model, the exchange constants are kept the same as in the undistorted lattice and the exchange energy for a magnetic spiral tilted by a β angle is proportional to β^2 . The magnetoelastic energy comes from the rotation of the magnetic moments (kept perpendicular to the wave vectors) and is a linear term in β [29]. Minimization of the total energy with respect to β reveals the occurrence of a tilt angle for the [1 0 0] and the [0 1 0] helices. The ε_{xy} shear thus introduces a new magnetoelastic term that favours the change of the moment directions for the D_1 and D_2 domains, even if this increases the exchange energy. Consequently, it favours a rotation of the magnetic propagation direction, assuming that the latter remains perpendicular to the plane that contains the magnetic moments. This mechanism has already been evoked [30] to describe the effect of a high magnetic field applied along non-cubic directions.

Thus, we have clearly demonstrated that tilting the magnetic propagation vectors κ_1 and κ_2 may allow for a reduction of either the exchange or magnetoelastic energy of the D_1 and D_2 magnetic domains. Besides, the D_3 domain is likely to vanish below a temperature where its energy cost becomes too high.

6. Magnetic structures in dhcp (001)Sm [11]

In the rare-earth series, Sm is an atypical element with respect to its crystal structure and its electronic and magnetic properties. At atmospheric pressure and for temperatures lower than 1197 K, it exhibits an exotic crystal structure with rhombohedral symmetry [31]: the hexagonal chemical cell can be described as a stack of nine close-packed planes. This ‘Sm-structure’ shows two sublattices of sites, with approximately hexagonal or cubic symmetry. As a consequence, two modulated magnetic phases, associated to the magnetic moments localized on the hexagonal and cubic sites, order successively below 106 K ($T_N^{\text{Sm,h}}$) and 13.8 K ($T_N^{\text{Sm,c}}$) [32–35]. The magnetic arrangement obeys the following rules:

- (i) The moments on both types of sites align along the c -direction.
- (ii) The magnetic order is ferromagnetic within the hexagonal planes.
- (iii) The hexagonal planes are antiferromagnetically coupled in a $(0 + + - - 0 + + - - \dots)$ sequence along the c -axis. The resulting propagation vector $\tau_h = (001.5)$.
- (iv) In each cubic plane, the moments form ferromagnetic rows parallel to one of the a -directions with a $+ + - - + + - - + + \dots$ sequence along the other two.
- (v) Although successive cubic planes are separated by two hexagonal planes (approximately 9 Å), they exhibit 3D ordering. The resulting propagation vector $\tau_c = (0.25\ 0\ 0.75)$.

Sm is known to undergo pressure- and/or temperature-induced crystallographic phase transformations to dhcp, hcp, bcc and fcc structures [36]. However, the magnetic behaviour of Sm in allotropes different from the ‘Sm-structure’ has been poorly studied up to now. In metastable dhcp Sm prepared under 40 kbar, a shift of the Néel ordering temperature has been detected by magnetization measurements

[37]. However, the magnetic structure of dhcp Sm has not yet been determined, probably because of the difficulty to prepare this phase, particularly as a single crystal.

The form of the Sm thin films makes it possible to perform neutron scattering measurements, even with natural Sm, because the single crystal nature of the sample maximizes the reflected intensity whilst its small thickness (a few hundred nanometers) minimizes absorption. In the following, we describe the first determination of the magnetic structure of dhcp Sm in a 750 nm dhcp (001)Sm film.

6.1 Hexagonal sites ordering

Neutron scattering performed at 300 K with the wave-vector transfer along (00 ℓ) and (10 ℓ) confirmed that the film had the dhcp structure (IN20 triple axis, ILL, France). No significant change in the intensity of the peaks was measured, and no additional reflections were observed on cooling the sample to 25 ± 1 K. At temperatures lower than 25 K, a clear increase in the intensity of all the peaks in the (10 ℓ) scan was observed. To demonstrate this transition, the scans recorded around the (100) reflection, above 130 K and below 4.5 K are illustrated in figure 8a; the thermal evolution of the integrated intensity measured for the same reflection is shown in figure 8b. The increase of the background observed at low temperature has been shown to be due to sample environment. No additional (00 ℓ) reflections have been observed at low temperature, confirming that the magnetic moments remain aligned along the c -axis.

The experimental ratios $R = I_{(1\ 0\ \ell)}/I_{(1\ 0\ 0)}$ (I is the integrated intensity) at 130 and 4.5 K have been shown to be in good agreement with calculated ratios, assuming, by analogy with the magnetic structure of bulk Sm, that:

- magnetic moments align along the c -axis,
- the coupling within each hexagonal plane is ferromagnetic,
- the coupling between hexagonal planes separated by a cubic plane is antiferromagnetic leading to $a + 0 - 0 + \dots$ sequence along the c direction (figure 9).

6.2 Cubic site ordering

Neutron scattering experiments were performed at 1.5 K in order to investigate the magnetic ordering of the cubic sites. A new magnetic peak around the (1.25 0 1) reflection with a very low intensity (10 counts/min) could be observed. This reflection can be attributed to magnetic ordering of the cubic sites as described below. However, because of the very low counting rate and the consequent prohibitive measurement time, it was not possible to undertake a detailed study of the cubic site ordering by neutron diffraction.

The high flux and low background available in the $\sigma - \pi$ configuration allowed the magnetic ordering of the cubic sites to be studied using RXMS (BM28 beamline at ESRF, France). It was established that the magnetic ordering on these sites occurs

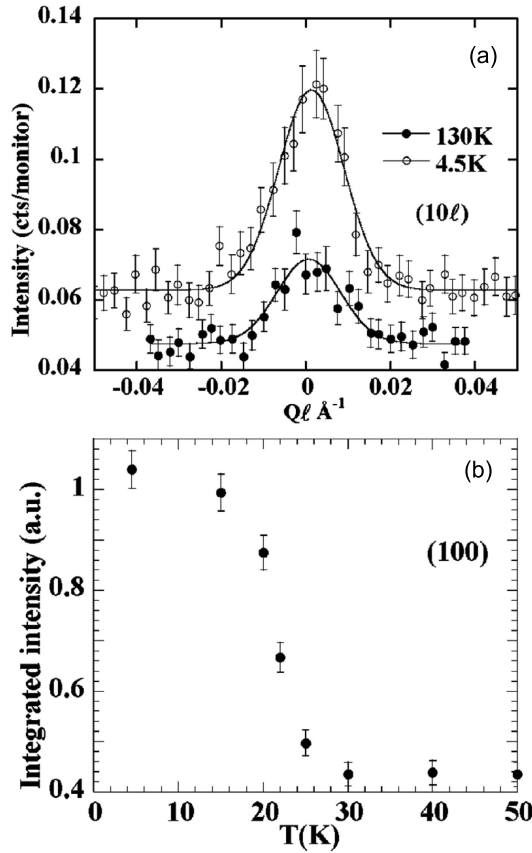


Figure 8. (a) Neutron scattering patterns at 130 and 4.5 K around the (100) reflection for a 750 nm dhcp (001)Sm film; (b) corresponding thermal evolution of the integrated intensity.

at 24 ± 1 K with the appearance of magnetic intensity in the $(0.25+0.5n \ 0 \ 2m+1)$ reflections (n and m are integers). Similar to the hexagonal sites, we established a model for the magnetic structure of the cubic sublattice by analogy with the bulk Sm. Two different structures can be considered. Both follows rules (i) and (iv) given above for the ‘Sm-structure’. Depending on how the basal planes couple, either a $\tau_{c1} = (0.25 \ 0 \ 1)$ or a $\tau_{c2} = (0.25 \ 0 \ 0.5)$ propagation vector could be expected. We observed several reflections corresponding to τ_{c1} , and none corresponding to τ_{c2} . So, the experimental results lead to the magnetic structure shown in figure 9. The calculated intensities are in qualitative agreement with the experimental data.

In summary, dhcp Sm has been shown to undergo a magnetic transition at about 25 K in which the hexagonal and cubic sites order nearly simultaneously. The ordering temperature of the hexagonal sites is perhaps lowered compared to bulk Sm because the hexagonal planes are isolated and the interaction between pairs of h-site-planes no longer occurs. Conversely, the ordering temperature of the cubic sites increases; this could be attributed to the fact that the interaction between

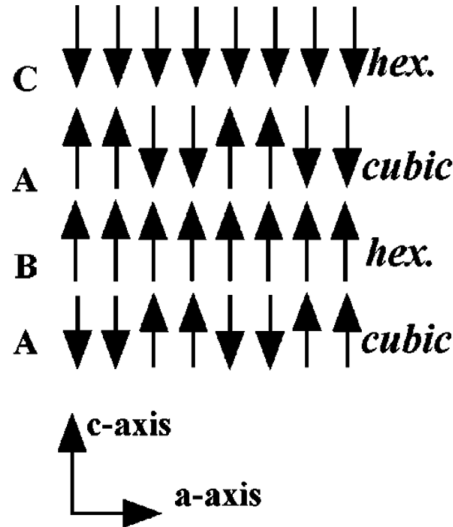


Figure 9. Sketch of the magnetic arrangement in dhcp Sm.

cubic planes is stronger than in bulk Sm because they are separated by only one instead of two hexagonal planes. The coupling between the two kinds of sites, even if it is weak, could also lead to convergence of the two magnetic transitions. The magnetic ordering in individual cubic planes, as well as in individual hexagonal planes, is the same as in bulk Sm. On the other hand, the magnetic ordering between the planes is modified (figure 9).

7. Conclusion

One of the main results presented in this paper is that the magnetic phase diagram of rare-earth metals can be tuned by epitaxy. Moreover, the separate roles of pseudomorphic strains and clamping to the substrate have been emphasized.

Epitaxial strains lead to a spectacular variation of Curie temperature (several tenth of degrees) in (001)Tb and (001)Dy films compared to bulk. This variation depends on the film thickness and the lattice parameter of the buffer, i.e. on the sign of the strain induced in the magnetic film.

The clamping to the thick substrate also participate to this variation of the Curie temperature in Tb and Dy films. Moreover, it induces a new magnetic order presenting a large wavelength modulation in (001)Tb films. This magnetic order can occur because magnetic anisotropy in Tb is smaller than in Dy in the helical-ferromagnetic transition temperature range. A new magnetic ordering has also been observed in (110)Eu epitaxial films as a consequence of a thickness- and temperature-dependent lattice clamping effect that distorts the Eu lattice at low temperature. Another important result is that Sm has been grown in a dhcp metastable phase using molecular beam epitaxy and that the magnetic structure of this dhcp Sm has been determined for the first time. The magnetic anisotropy and

the magnetic order in a given basal plane are similar to the bulk ones. However, the 3D magnetic ordering and the ordering temperature are modified compared to the bulk. This magnetic structure can be understood from crystal symmetry considerations.

References

- [1] M R Fitzsimmons *et al*, *J. Magn. Magn. Mater.* **271**, 103 (2004)
- [2] J Jensen and A R Macintosh, *Rare earth magnetism* (Oxford Science Publications, Oxford, Great Britain, 1991)
- [3] K Dumesnil *et al*, *Phys. Rev.* **B54**, 6407 (1996)
- [4] K Dumesnil, C Dufour, Ph Mangin, G Marchal and M Hennion, *Europhys. Lett.* **31**, 43 (1995)
- [5] K Dumesnil, C Dufour, Ph Mangin and G Marchal, *Phys. Rev.* **B53**, 11218 (1996)
- [6] K Dumesnil, C Dufour, Ph Mangin, G Marchal and M Hennion, *Phys. Rev.* **B54**, 6407 (1996)
- [7] C Dufour, K Dumesnil, A Mougine, Ph Mangin, G Marchal and M Hennion, *J. Phys.: Condens. Matter* **9**, L131 (1997)
- [8] C Dufour, K Dumesnil, Ph Mangin and M Hennion, *J. Phys.: Condens. Matter* **11**, L497 (1999)
- [9] S Soriano, K Dumesnil, C Dufour, T Gourieux, Ph Mangin, J A Borchers and A Stunault, *Phys. Rev.* **B71**, 092409 (2005)
- [10] S Soriano, C Dufour, K Dumesnil, J A Borchers and Ph Mangin, *Appl. Phys. Lett.* **85**, 4636 (2004)
- [11] C Dufour, K Dumesnil, S Soriano, Ph Mangin, P J Brown, A Stunault and N Bernhoeft, *Phys. Rev.* **B66**, 094428 (2002)
- [12] J Kwo, M Hong and S Nakahara, *Appl. Phys. Lett.* **49**, 319 (1986)
- [13] C Dufour, K Dumesnil, S Soriano, D Pierre, Ch Senet and Ph Mangin, *J. Crystal Growth* **234**, 447 (2002)
- [14] S Soriano, K Dumesnil, C Dufour and D Pierre, *J. Crystal Growth* **265**, 582 (2004)
- [15] M K Wilkinson, W C Koelher, E O Wollan and J W Cable, *J. Appl. Phys.* **32**, 488 (1961)
- [16] J W Cable, E O Wollan, W C Koelher and M K Wilkinson, *Phys. Rev.* **140**, A1896 (1965)
- [17] B Coqblin, *The electronic structure of the rare earth metals and alloys: The heavy rare earth* (Academic, London, 1977)
- [18] H B Callen and E Callen, *Phys. Rev.* **A139**, 455 (1965)
- [19] W C Koelher, E O Wollan and J W Cable, *J. Appl. Phys.* **34**, 1335 (1963)
- [20] W C Koelher, *J. Appl. Phys.* **36**, 1078 (1965)
- [21] P M Gehring, L Rebelsky, D Gibbs and G Shirane, *Phys. Rev.* **B45**, 243 (1992)
- [22] R M Bozorth and J H Van Vleck, *Phys. Rev.* **118**, 1493 (1960)
- [23] N G Nereson, C E Olsen and G P Arnold, *Phys. Rev.* **135**, A176 (1964)
- [24] A H Milhouse and K A McEwen, *Solid State Commun.* **13**, 339 (1973)
- [25] R L Cohen, S Hüfner and K W West, *Phys. Rev.* **184**, 263 (1969)
- [26] A S Bulatov and O V Kovalev, *Sov. Phys. Solid State* **30**, 266 (1988)
- [27] H U Aström *et al*, *J. Magn. Magn. Mater.* **104–107**, 1507 (1992)
- [28] E F Bertaut, *J. Phys. Chem. Solids* **21**, 256 (1961)
- [29] A E Clark, *Handbook on the physics and chemistry of rare earths* edited by Gschneider

- and Eyring (North Holland Publishing, Amsterdam, The Netherland, 1979) vol. 2, chap. 15
- [30] K A McEwen *et al*, *Phys. Rev. Lett.* **30**, 287 (1973)
 - [31] A H Daane, R E Rundle, H G Smith and F H Spedding, *Acta Crystallogr.* **7**, 534 (1954)
 - [32] W C Kohler and R M Moon, *Phys. Rev. Lett.* **29**, 1468 (1972)
 - [33] S L Lee *et al*, *J. Magn. Magn. Mater.* **127**, 145 (1993)
 - [34] K Dumesnil, C Dufour, Ph Mangin, M Hennion and P J Brown, *Phys. Rev.* **B60**, 10743 (1999)
 - [35] K Dumesnil, C Dufour, Ph Mangin and A Stunault, *J. Phys.: Condens. Matter* **12**, 3091 (1999)
 - [36] B R Coles, *J. Less Common Metals* **77**, 153 (1981)
 - [37] A Jayaraman and R C Sherwood, *Phys. Rev.* **134**, A692 (1964)